ilmedia

TECHNISCHE UNIVERSITÄT
ILMENAU

Stephan Gorges, Hartmut Brauer, Marek Ziolkowski, Matthias Carlstedt, Konstantin Weise, Reinhard Schmidt, Judith Mengelkamp

Motion-induced eddy current testing of composite materials

URN: urn:nbn:de:gbv:ilm1-2016200182

Original published in:

The e-journal of nondestructive testing & ultrasonics. - Kirchwald : NDT.net. - Bd. 21.2016, 7, insges. 9 S.

ISSN (online): 1435-4934
URL: http://ndt.net/?id=19726
[*Visited:* 2016-10-01]

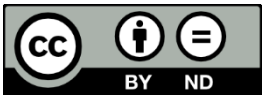

This work is licensed under a Creative Commons Attribution-NoDerivs 3.0 Unported License
https://creativecommons.org/licenses/by-nd/3.0/

TU Ilmenau | Universitätsbibliothek | ilmedia, 2016
http://www.tu-ilmenau.de/ilmedia

Motion-induced Eddy Current Testing of Composite Materials

Stephan GORGES [1], Hartmut BRAUER [1], Marek ZIOLKOWSKI [1, 2], Matthias CARLSTEDT [1], Konstantin WEISE [1], Reinhard SCHMIDT [1], Judith MENGELKAMP [1]
[1] Technische Universität Ilmenau, Ilmenau, Germany
[2] West Pomeranian University of Technology, Szczecin, Poland

Contact e-mail: stephan.gorges@tu-ilmenau.de

Abstract. Modern composite materials are gaining more and more importance in mechanical engineering. Due to the complex structure of most of these materials, traditional NDT methods do not satisfy the measurement requirements.

In this paper we address the capabilities and limitations of the non-destructive testing method of motion-induced eddy currents for (non-ferromagnetic) composite materials.

The specimen moves with constant velocity through a magnetic field, which is created by a fixed permanent magnet.

The interaction of induced eddy currents and the primary magnetic field results in the Lorentz force acting on the specimen. Due to the third Newton law, the reaction force acts on the magnet system itself and is measured in all three spatial dimensions.

Every force component has a characteristic profile for a certain defect-free specimen. Anomalies in the specimen affect the eddy currents due to variations of local conductivity. These deviations influence the measured force profiles from which the location, size and type of the defect in the specimen may be determined.

Two types of magnet systems have been applied: a cylindrical magnet and a radial Halbach array with a ferromagnetic disc. The cylindrical magnet produces a dipole-like field, whereas the Halbach array with the additional disc creates a field concentrated right below the magnet system.

Experiments show, that the Halbach array is very well suited for thin specimens. The defect response signal is higher due to the stronger eddy currents caused by the focused magnetic field.

Two different types of composite materials have been experimentally tested: Carbon fibre reinforced plastic (CFRP) and glass laminate aluminium reinforced epoxy (GLARE). For CFRP four samples were fabricated, whereas one was tested. For GLARE two samples were used with defects in different depth.

1 Introduction

Lorentz force Eddy Current Testing (LET) is a novel approach for Nondestructive Testing (NDT) of conductive materials. Especially for modern composite materials common methods may not suite the special requirements of these materials. LET is a promising technique which utilizes various physical effects to test the material for defects or anomalies [1].

In this paper the basic physical effects of LET are presented and the used measurement setup is described. Different types of samples with various defects and defect depths

License: http://creativecommons.org/licenses/by-nd/3.0/

are presented. The magnetic fields of two magnet systems have been studied preliminary. Using these magnet systems LET has been performed on the specimens. The resulting graphs show the performance of the magnet systems with respect to the defect type and depth.

2 Basic Principle of LET

In LET, the specimen is required to be non-ferromagnetic ($\mu = \mu_0$) and conductive. An isotropic conductivity σ is assumed. The specimen moves with a constant velocity $\mathbf{v}$ through a stationary magnetic field $\mathbf{B}_0$ created by a magnet system, see Fig. 1. [1]

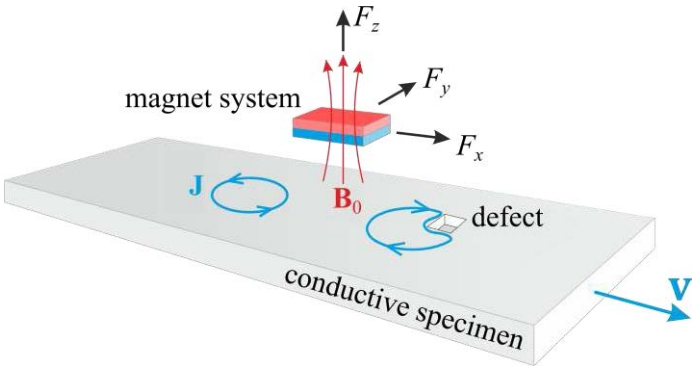

Fig. 1. Basic principle of LET

Assuming quasistatic behaviour and neglecting the secondary magnetic field produced by the eddy current density $\mathbf{J}$ induced in the specimen [2], the $\mathbf{J}$ can be directly described by Ohm's law for moving conductors as:

$$\mathbf{J} = \sigma(-\nabla\varphi + \mathbf{v} \times \mathbf{B}_0) \tag{1}$$

where φ is the scalar electric potential and $\mathbf{v} = [v, 0,0]^{\mathrm{T}}$. The eddy currents interacting with the primary magnetic field $\mathbf{B}_0$, therefore the Lorentz force $\mathbf{F}_{\mathrm{L}}$ acts on the specimen. Due to Newton's third law, the opposite force $\mathbf{F}$ will act on the magnet system:

$$\mathbf{F} = \left[F_x, F_y, F_z\right]^{\mathrm{T}} = -\mathbf{F}_{\mathrm{L}} = -\int_V \mathbf{J} \times \mathbf{B}_0 \, dV \tag{2}$$

where V is the volume of the specimen. This force $\mathbf{F}$ is constant, as long as σ and $\mathbf{v}$ are not changing. For specimens with defects (a region in the volume with $\sigma_{\mathrm{Defect}} < \sigma$), the magnitude of the force $\mathbf{F}$ is reduced, which can be measured [3].

3 Experimental setup

3.1 Measuring Instrumentation

For the experiments the BASALT-C MMP-15 [4] was used (Fig. 2). This device consists of the mechanical system and the control cabinet. The mechanical system is set on a granite block with high mass to increase the inertia, thereby reducing external influences on the force sensing unit. On the block, a linear direct drive is mounted to realize movement in x-direction. The investigated specimen is mounted on the slide of this drive. The direct drive is able to accelerate and deaccelerate with up to 50m/s² and maintain a constant velocity with very little deviation.

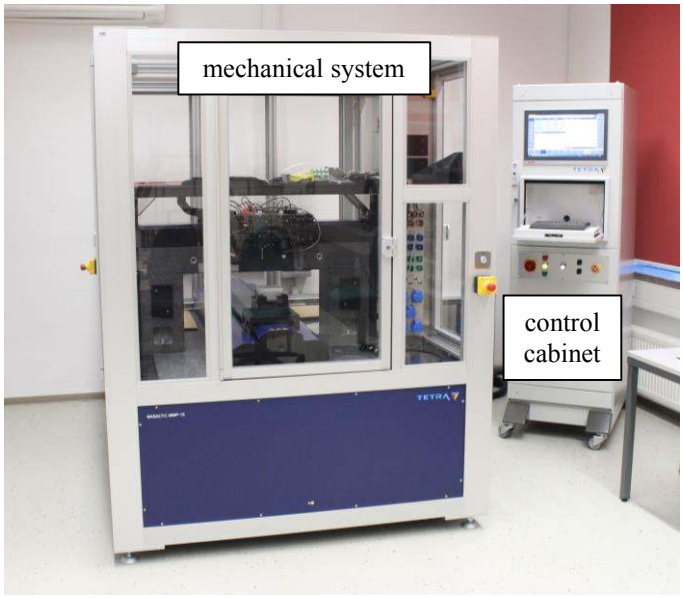

Fig. 2. BASALT-C MMP-15

On the block a granite portal is installed which spans over the linear drive. On the portal spindle drives in z- and y-direction are mounted. The one end of the force sensor is fixed to the z-slide while on the other end the magnet system is attached. Thus, the magnet system can be positioned freely above the surface of the specimen. The setup is shown in Fig. 3. All drives are controlled via a panel PC located in the control cabinet. The measurement data is also gathered by this computer. Integrating these two tasks into one device allows programming of complex measurement tasks using G-code. [4]

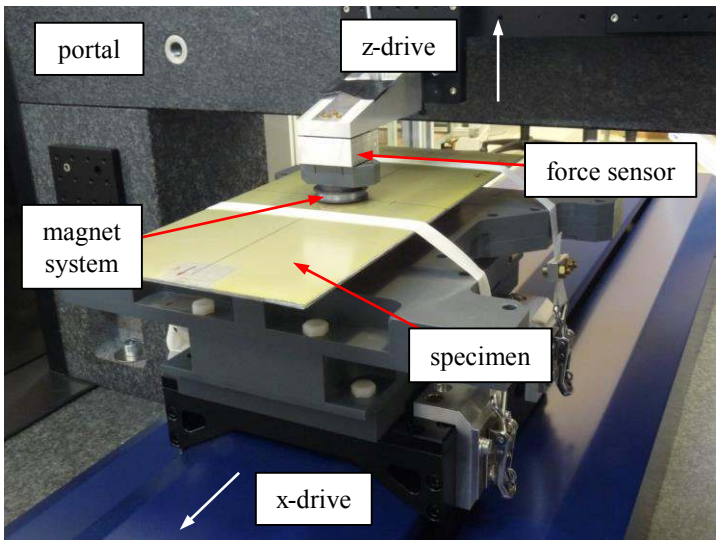

Fig. 3. Measurement setup for LET

3.2 LET Measuring Procedure and Force Sensor

To perform LET experiments, a specimen is mounted on the x-drive. The magnet system is positioned at a desired y-coordinate above the specimen. The z-coordinate is set by moving the magnet system down, until a specified gap to the specimen (lift-off distance δ) is left. The specimen starts to accelerate from a start position outside the magnetic field of the magnet system. After reaching the desired velocity v the PC starts to collect the measured force

and positional data with a sampling frequency f_S. After leaving the magnetic field, the specimen is stopped and moved back to the starting position. Now, the scan can be repeated at the same or a different y-coordinate.

The force sensor used during measurements is the K3D40 from ME-Meßsysteme GmbH [5]. It is a triaxial sensor with ± 2N nominal force in all three directions. As stated above, it is mounted to the z-drive. On the other end a plate with a notch is mounted. The counterpart of this notch is part of the magnet system mounting bracket, which enables to mount the magnet system at a reproducible position.

3.3 Measuring Procedure for Magnetic Fields and Applied Magnet Systems

To measure the magnetic field formed by the applied magnet system, a Hall probe is fixed to the z-slide. Thereby, the probe can be moved in the yz-plane. The magnet system is fixed to the x-slide, hence the Hall probe can be positioned in all three spacial dimension in relation to the magnet system. The probe is moved along a grid and takes a reading at every gridpoint.

The AS-N3DM probe by Projekt Elektronik Mess- und Regelungstechnik GmbH [6] is used to measure the magnetic field of the magnet system. It is a triaxial Hall probe with a range of ± 2T.

Two magnet systems have been applied: A longitudinal magnetized cylindrical magnet (Ø22.5mm, height: 17.6mm) and a radial magnetized Halbach array (Ø24.8mm, height: 14.5mm) with a high-permeable disc made of iron-cobalt alloy VACOFLUX 50 [7]. Both magnet systems are results if the optimization procedure presented in [8]. The structure of the Halbach is shown in Fig. 4 and 5.

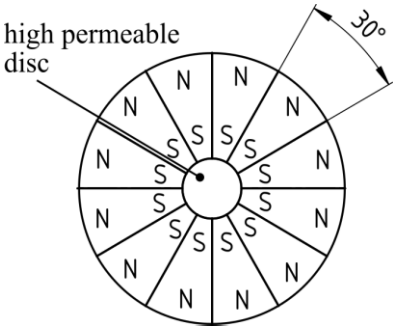

Fig. 4. Magnetization structure of the Halbach array (bottom view)

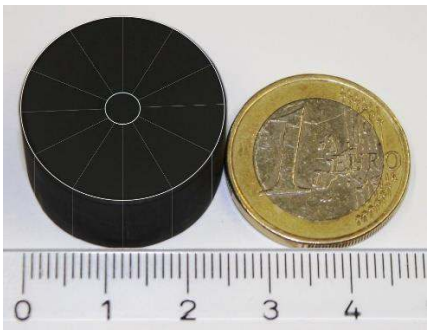

Fig. 5. Size comparison of the Halbach array to a 1€ coin

The idea behind the Halbach structure is to increase the magnetic flux density in the vicinity of the magnet system. Because of this focusing effect, the Halbach magnet system is expected to perform better for small defects and defects close to the surface of the specimen.

3.4 Magnetic Fields of the Cylindrical Magnet and the Halbach Array

Fig. 6 shows the magnetic flux density components of the used magnet systems. The top pictures show the measured data for the Halbach array, whereas the bottom pictures show data for the cylindrical magnet. The x-component is not shown because it is very similar to the y-component, only rotated around the z-axis by 90°. The magnetic flux density is measured at a distance of 1mm from the housing of the probe to the surface of the magnet system.

The B_z-component produced by the cylindrical magnet forms a circular plateau, whereas for the Halbach array it is cone-shaped. The plateau is only half ($\approx 400\text{mT}$) as strong as the cone tip of the Halbach array ($\approx 800\text{mT}$). It can be observed that the contour lines for the Halbach array are much denser than for the cylindrical magnet. A similar behaviour can be observed in the B_y graphs. Thus, it can be noted that the magnetic flux density $\mathbf{B}_0$ below the Halbach array is much more focused than for the cylindrical magnet. According to (1) and (2) a specimen moved under the Halbach array should result in a higher measured Lorentz force **F**.

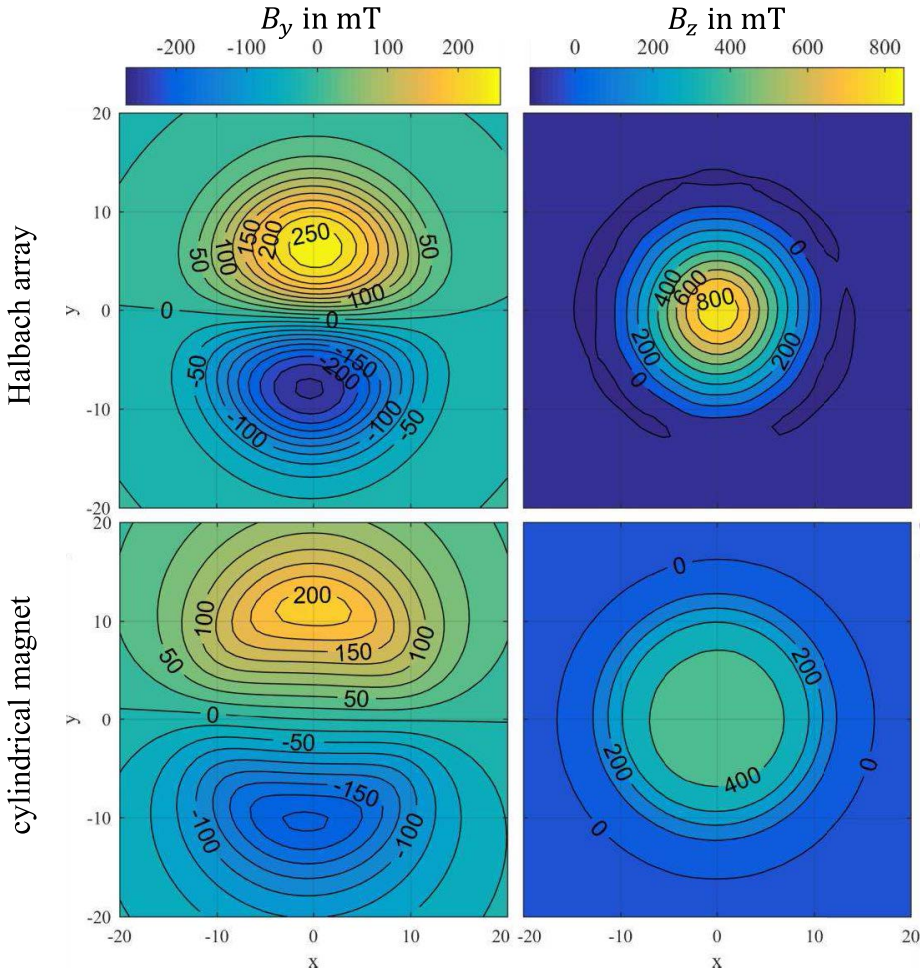

Fig. 6. Comparison of magnetic flux density components of the Halbach array and the cylindrical magnet

3.5 Types of Specimens

3.5.1 Glass laminate aluminium reinforced epoxy (GLARE)

GLARE is made of thin stacked aluminium sheets with glass fibre laminated in-between the sheets. It is mainly used in aerospace because of its mechanical properties and low specific weight [9, 10]. The layer structure can be seen in Fig. 7. Typically GLARE is tested nondestructively with ultrasonic [11] or thermography [12].

The two GLARE specimens shown in Fig. 8 were used in this study. Both specimens are 350mm by 150mm and made of 5 aluminium sheets, each 0.4mm thick, with 0.25mm glass fibre laminate between the sheets, resulting in a total thickness of the specimen of 3mm. Both specimens have a slot ($10\text{mm} \times 1\text{mm}$) and a drilled hole ($\emptyset$ 2mm) at the marked spots in one of their aluminium layers. Specimen 1 has the defects in aluminium layer 3 (defect

depth: 1.3mm) and specimen 2 in layer 2 (defect depth: 0.65mm), counted from the top layer.

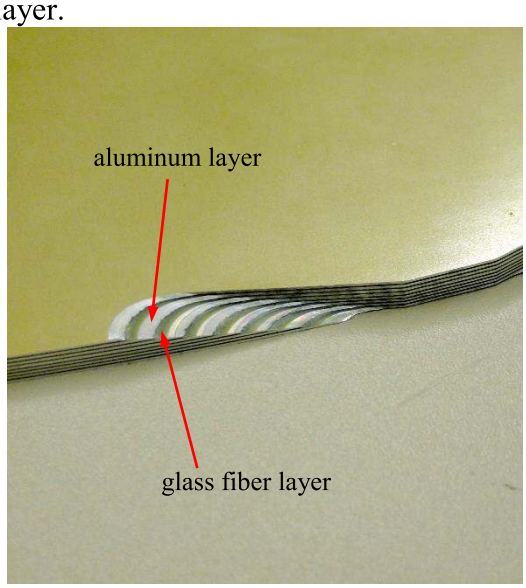

Fig. 7. Layer structure of GLARE (8 aluminium sheets with 7 glass fibre layers inbetween)

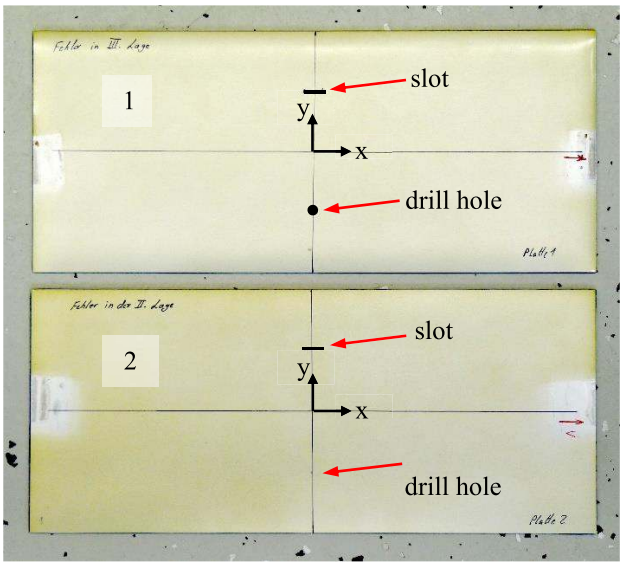

Fig. 8. Two sample specimens of GLARE with marked defects

3.5.2 Carbon fibre reinforced polymer (CFRP)

CFRPs are very popular nowadays when there are high demands on the mechanical properties of a part. Most CFRP parts are made by laminating different types of carbon fibre fabrics on another. This type of composite material has one of the highest strength-to weight ratios available. Therefore, CFRPs are mostly applied in aerospace, automotive and sports. Because the fibres are electric conductors, nondestructive eddy current based methods have been already successfully applied on CRFPs [13].

Four different specimens of CFRP for testing with LET were fabricated. All have the same size of 275mm × 275mm. For specimen 1, 2 and 3 the same unidirectional non-crimped fabric was used. For specimen 4 a plain weave was used. Detailed information about the specimens are shown in Table 1.

Table 1. Information about the fabrication and layering structure of the CFRP specimens

Specimen no.	1	2	3	4
	unidirectional	bidirectional	quasiisotropic	fibre fabric
layering structure				
specific fabric weight	620 g/m²	620 g/m²	620 g/m²	400 g/m²
layer directions	0°	0°, 90°	-45°, 0°, 45°, 90°	plain weave
number of layers	29	29	32	40
total thickness	20 mm	20 mm	22 mm	20 mm
estimated fibre vol.%	45	45	45	45

According to [14], the eddy currents increase when there are more contact points between the fibres in the laminate. Since specimen 4 is made from a weave, where the fibres cross each other inside the single layers and therefore a lot of contact points should exist, this specimen is used in the following study.

4 Results and Discussion

All presented LET experiments are performed with a specimen velocity of $v = 200\text{mm/s}$ and a lift-off of $\delta = 1\text{mm}$. For GLARE, the y-coordinate was incremented by 0.5mm over the 150mm width of the specimen. For every y-coordinate 25 measurements were performed, and next averaged to reduce random errors in the data. For the CFRP specimen measurements at 5 different y-coordinates over the middle of the specimen were carried out. In this case the goal was not to find defects but rather only to detect the specimen structure with LET.

4.1 Comparison Cylindrical Magnet – Halbach Array

Both the cylindrical magnet and the Halbach array are used to scan the GLARE specimen 1. The coordinate system is set in the centre of the specimen. Figures 9 and 10 show the x- and z-component of the measured forces (drag and lift force) across the centreline of the specimen. The side force F_y is of no interest for these studies.

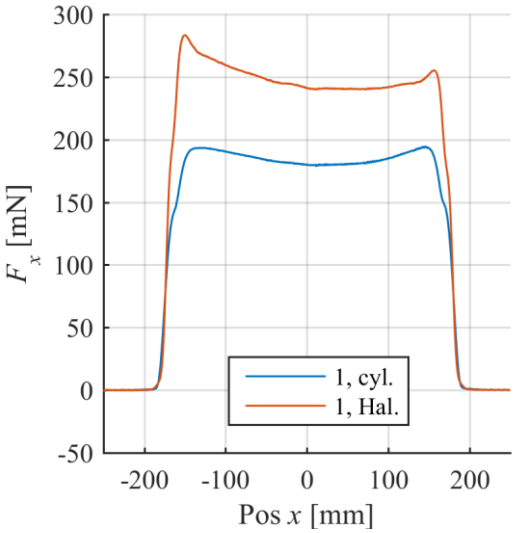

Fig. 9. Measured x-force (drag force)

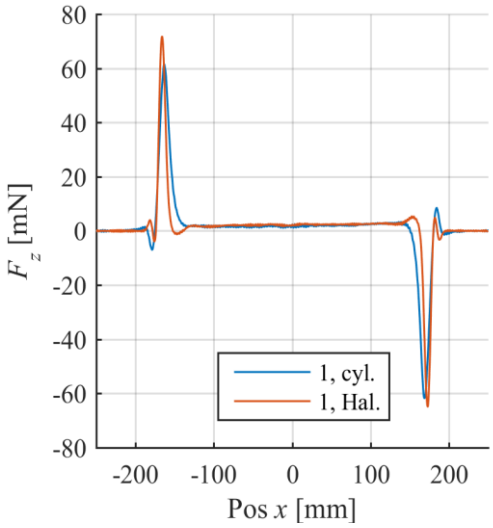

Fig. 10. Measured z-force (lift force)

On the centreline of the specimen ($y = 0$), no defect is present. The leading edges of the specimen entered the magnet field at $x \approx -175\text{mm}$. The trailing edge left the magnet field at $x \approx 175\text{mm}$. F_z has a positive and negative peaks at these positions, whereas F_x rises to a plateau and drops back to zero. According to theory, the plateau should be constant since no parameter changes over the specimen. Fig. 9 shows that the plateau has a dent, which originates from an uneven surface and therefore a change in the lift-off distance. Both the cylinder magnet and the Halbach array show this behaviour.

For the Halbach array, the maximum forces are clearly higher and the general force profile is sharper comparing to the cylindrical magnet. This is the result of the focused magnetic flux density produced by the Halbach array.

4.2 Comparison of GLARE Defect Depth

The following figures present the comparison of the resulting force acting on the magnet in dependence of the defect depth. Here only the results for the Halbach array are shown. The plots are cropped to x-range $[-50\text{mm}, 50\text{mm}]$. The solid lines correspond to the slot defect while the dotted lines to the drill hole defect. The results for GLARE specimen 1 and GLARE specimen 2 are depicted with red and green colours, respectively.

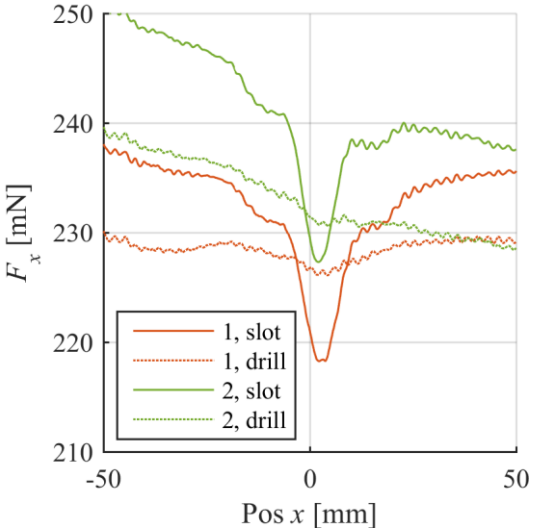

Fig. 11. F_x response signals in the vicinity of the defects

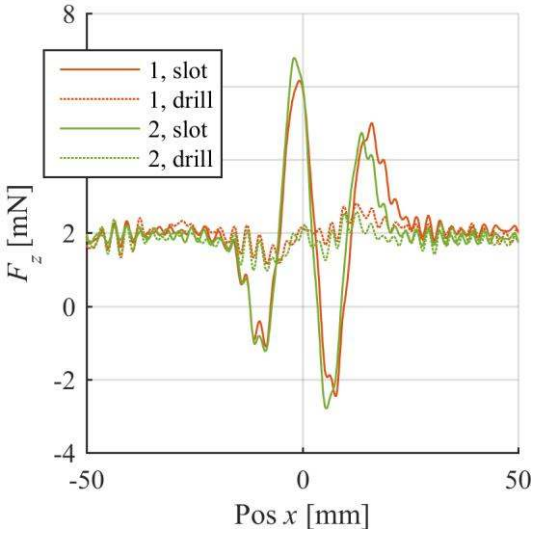

Fig. 12. F_z response signals in the vicinity of the defects

From Fig. 11, it can be noted that the deformed surface deviations influences F_x a lot and makes it difficult to find out, where the deeper defect is. In Fig. 12, it can be observed that for the specimen 2 the deflections caused by the slot defect are a little bit larger, than for the specimen 1. Since the specimen 2 has the defects in the second aluminium layer, they are 0.65mm closer to the magnet system then in specimen 1 and should indeed result in a stronger deflection in the force. The drill hole is hardly distinguishable in the z-component. From the drill hole signals it cannot be concluded which the deeper defect is, since the noise oscillations in the signal are too high.

4.3 CFRP and non-conductive PVC

In this study the CFRP specimen 4 (plain weave) is used in combination with the Halbach array and compared to a non-conductive PVC bar. The recorded signals are filtered with a running average filter (window width: 17ms). The resulting force signals are presented in Fig. 13 and 14. It can be observed that the noise in relation to the signal is very large, therefore the F_x-component cannot be interpreted. Surprisingly, the F_z signal has a plateau, with the length corresponding with the specimen length, i.e. PVC: 250mm, CFRP: 275mm. Because the non-conductive PVC bar creates also a plateau in the measured force profile, the observed

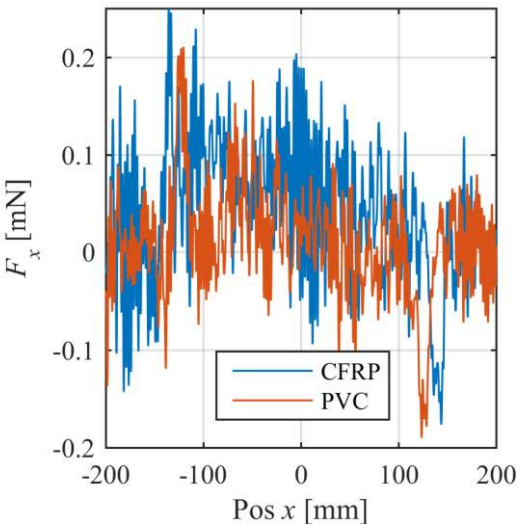

Fig. 13. Filtered F_x-signal for CFRP and PVC

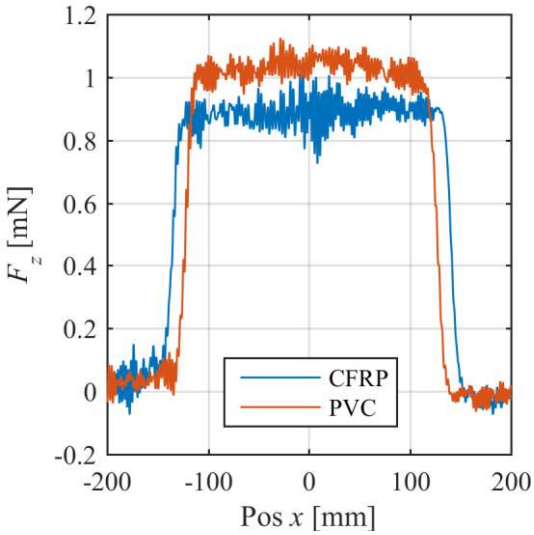

Fig. 14. Filtered F_z-signal for CFRP and PVC

force is not the result of eddy currents induced in the specimen. Probably aerodynamic effects act on the magnet system and result in a measured force.

5 Conclusion

In this paper, recent measurement experiments in Lorentz force eddy current testing (LET) are presented. The testing setup and procedure are described. The magnetic field of the two magnet systems, i.e. the Halbach array and the cylindrical magnet, are measured, compared and evaluated. The effects of the various magnet systems on LET are demonstrated. The advantages of the Halbach array in detection of very small defects in thin specimens are exploited. Furthermore, a carbon fibre specimen is investigated. It is demonstrated that the investigation of CFRP is still a big challenge for LET.

6 Acknowledgement

This work was supported by Deutsche Forschungsgemeinschaft (DFG) through the VIP-project.

7 References

[1] Brauer, H., Porzig, K., Mengelkamp, J., Carlstedt, M. et al., Lorentz force eddy current testing: a novel NDE-technique. COMPEL 2014, 33, 1965–1977.
[2] Zec, M., Uhlig, R. P., Ziolkowski, M., Brauer, H., Fast Technique for Lorentz Force Calculations in Non-destructive Testing Applications. IEEE Trans. Magn. 2014, 50, 7003104(1–70031044.
[3] Carlstedt, M., Porzig, K., Uhlig, R. P., Zec, M. et al., Application of Lorentz force eddy current testing and eddy current testing on moving nonmagnetic conductors. International Journal of Applied Electromagnetics and Mechanics 2014, 45, 519–526.
[4] TETRA Gesellschaft für Sensorik, Robotik und Automation mbH, Betriebsanleitung: BASALT®-C MMP-15.
[5] ME-Meßsysteme GmbH, Datenblatt: Mehrachsen-Kraftsensor K3D40, 2014.
[6] Projekt Elektronik Mess- und Regelungstechnik GmbH, Datenblatt: 3D-Magnetfeldsonden AS-N3DM und AS-L3DM, 2015.
[7] VACUUMSCHMELZE GmbH & Co. KG, Hanau, Weichmagnetische Kobalt-Eisen-Legierungen: Vacoflux 48, Vacoflux 50 Vacodur 49, Vacodur 50, Vacodur S Plus, Vacoflux 17, Vacoflux 18 HR, Vacoflux 9 CR, Hanau 2001.
[8] Weise, K., Schmidt, R., Carlstedt, M., Ziolkowski, M. et al., Optimal Magnet Design for Lorentz Force Eddy Current Testing. IEEE Trans. Magn. 2015, 51, 6201415(1–62014115.
[9] Thomas Beumler, Flying GLARE: A contribution to aircraft certification issues on strength properties in non-damaged and fatigue damaged GLARE structures. Dissertation, Delft 2004.
[10] Guocai Wu, J.-M. Yang, The Mechanical Behavior of GLARE Laminates for Aircraft Structures. JOM, 2005, 72–79.
[11] W. Haase, A. Maurer, Latest developments on industrial ultrasonic testing of aircraft components. Proceedings of the World Conference on Non-Destructive Testing 2004, 225–236.
[12] Carosena Meola, Giovanni Maria Carlomagno, Antonino Squillace, Antonio Vitiello, Non-destructive evaluation of aerospace materials with lock-in thermography. Engineering Failure Analysis 2006, 380–388.
[13] Henning Heuer, Martin H. Schulze, Norbert Meyendorf, High Resolution Inspection of Carbon Fiber Materials by Eddy Current Techniques. 2nd Intern. Symp. NDT in Aerospace 2010, A3.
[14] Xin Li, Eddy Current Techniques for Non-destructive Testing of Carbon Fibre Reinforced Plastic (CFRP), Manchester 2012.